RESEARCH ARTICLE

ASYMMETRIC CATALYSIS

Generality-oriented optimization of enantioselective aminoxyl radical catalysis

Jonas Rein[1]†, Soren D. Rozema[2]†, Olivia C. Langner[2]‡, Samson B. Zacate[1]‡, Melissa A. Hardy[3], Juno C. Siu[1], Brandon Q. Mercado[2], Matthew S. Sigman[3]*, Scott J. Miller[2]*, Song Lin[1]*

Catalytic enantioselective methods that are generally applicable to a broad range of substrates are rare. We report a strategy for the oxidative desymmetrization of *meso*-diols predicated on a nontraditional catalyst optimization protocol by using a panel of screening substrates rather than a singular model substrate. Critical to this approach was rational modulation of a peptide sequence in the catalyst incorporating a distinct aminoxyl-based active residue. A general catalyst emerged, providing high selectivity in the delivery of enantioenriched lactones across a broad range of diols, while also achieving up to ~100,000 turnovers.

Substrate generality is a long-standing aim in the field of enantioselective catalysis (*1*–*3*). Even so, specificity-oriented optimization has been broadly adopted in the field, resulting in many catalysts that are tailored for one model substrate but often exhibit diminished selectivity upon surveying a diverse substrate scope (Fig. 1A) (*4*). To address the limited transferability frequently encountered in asymmetric catalysis, we envisioned an optimization strategy with generality as the primary objective in catalyst development. This strategy requires parallel screening of a large, diverse catalyst library against a judiciously selected panel of model substrates that represent the chemical space of the target substrate class, rather than a singular substrate. Such an approach is reminiscent of the "one-pot multi-substrate" method to increase screening throughput (*5*–*8*). However, this pooled-substrate method introduces challenges in chemical compatibility and product analysis and thus has seen limited implementation in catalyst development.

Recently, Jacobsen and co-workers reported a pooled-product method for enantioselectivity analysis, which enabled high-throughput evaluation of the generality of known catalysts in the context of an asymmetric Pictet-Spengler reaction (*4*). Our interest focused on advancing the notion of enhanced substrate breadth in the context of previously elusive transformations by using a new catalytic platform. Toward this objective, we envisioned that small synthetic, catalytic peptides would be well suited for such a study, given the modularity of their constituent amino acids and their synthetic accessibility, which provides a strong foundation for a generality-driven optimization campaign (*9*). Peptide optimization can also bear a resemblance to the venerable directed evolution of enzymes through survey of multidimensional catalyst space (*10*, *11*). Our study combined the vast amount of catalyst space surveyed with a computationally informed representative substrate space, yielding information-rich data that can be used for subsequent catalyst optimization. We investigated this strategy in an underexplored area in asymmetric synthesis: enantioselective aminoxyl radical catalysis (*12*).

Aminoxyl radicals are a class of persistent open-shell molecules that have found broad applications in organic synthesis (*13*). They are excellent catalysts for the oxidation of various functional groups such as alcohols, amines, and alkenes through intermediate oxoammonium ions (*13*–*18*). In contrast to the vast number of reactions known to be catalyzed by aminoxyl radicals, enantioselective variants remain rare, hampered by a dearth of synthetically accessible and tunable catalysts. Foundational work by the group of Bobbitt and recent advances by Iwabuchi and co-workers among others provided salient precedents in asymmetric alcohol oxidation (Fig. 1B) (*19*–*22*). Nevertheless, these catalysts require lengthy synthetic preparation and lack the structural modularity needed for generality-oriented optimization; accordingly, substrate scope for these efforts suffers from diminished enantioselectivities beyond a handful of similar substrates. Toniolo and co-workers demonstrated that oxoammonium ions are compatible within peptidic frameworks and observed the kinetic resolution (KR) of a singular alcohol substrate with modest selectivities [relative rate constant (k_{rel}) < 3] (*12*).

We hypothesized that incorporation of an achiral aminoxyl moiety into diverse peptide-based scaffolds would enable rapid substrate exploration within the reaction space accessible to chiral aminoxyl catalysis. Accordingly, we designed and synthesized an aminoxyl monomer (**Azc-OMe**) (Fig. 1C); the azaadamantyl aminoxyl framework was selected for its excellent activity in catalytic alcohol oxidation resulting from its high oxidation potential, enhanced steric accessibility compared with that of monocyclic aminoxyls, and conformational rigidity (*23*). Additionally, a methyl ester adjacent to the aminoxyl residue enables rapid incorporation into peptide frameworks with the aminoxyl moiety proximal to the chiral functionality. This monomer design allowed for the synthesis of >70 chiral aminoxyl peptides. We report the development of the enantioselective desymmetrization of *meso*-diols, for which a generality-oriented optimization campaign led to an aminoxyl-based oligopeptide catalyst that delivers high selectivity for accessing structurally diverse enantioenriched lactones.

Initial studies using a traditional optimization strategy

We began our study with the desymmetrization of *meso*-diols (Fig. 2A), which proceeds with an initial oxidation of one of the enantiotopic hydroxyl groups, followed by cyclization through attack of the second hydroxyl group on the incipient aldehyde to furnish an intermediate chiral lactol (**H**). A second oxidation then delivers a lactone (**L**). Chiral lactones are valuable and versatile building blocks in organic and polymer synthesis as well as medicinal chemistry. Although methods are available for synthesizing specific types of enantioenriched lactones, a broadly applicable approach that is compatible with a wide range of substrate structures, ring sizes, and substitution patterns remains elusive and desirable. In particular, few reports achieved chiral lactone synthesis through the oxidative desymmetrization of readily available *meso*-diols; these methods—which use either a transition metal (iridium or ruthenium) (*24*, *25*) or organocatalysis (*19*, *26*–*28*)—show limited substrate diversity and/or moderate enantioselectivity.

We initially used a traditional optimization approach by screening a collection of aminoxyl-embedded peptide catalysts in the oxidation of 1,4-diol **S1**, using trichloroisocyanuric acid (TCCA) as a terminal oxidant and sodium bicarbonate as a base (*20*, *21*). This effort yielded peptide **P1**, which provided lactone **L1** with substantial enantioselectivity [75% enantiomeric excess (*ee*)]. However, **P1** showed diminished selectivity when tested against an array of additional 1,4-diols that display a variety of steric and electronic profiles, giving a median ee (ee_{med}) of only 16% (Fig. 2E, column **P1**). This

[1]Department of Chemistry and Chemical Biology, Cornell University, Ithaca, NY 14853, USA. [2]Department of Chemistry, Yale University, New Haven, CT 06520, USA. [3]Department of Chemistry, University of Utah, Salt Lake City, UT 84112, USA.
*Corresponding author. Email: songlin@cornell.edu (S.L.); scott.miller@yale.edu (S.J.M.); matt.sigman@utah.edu (M.S.S.)
†These authors contributed equally to this work.
‡These authors contributed equally to this work.

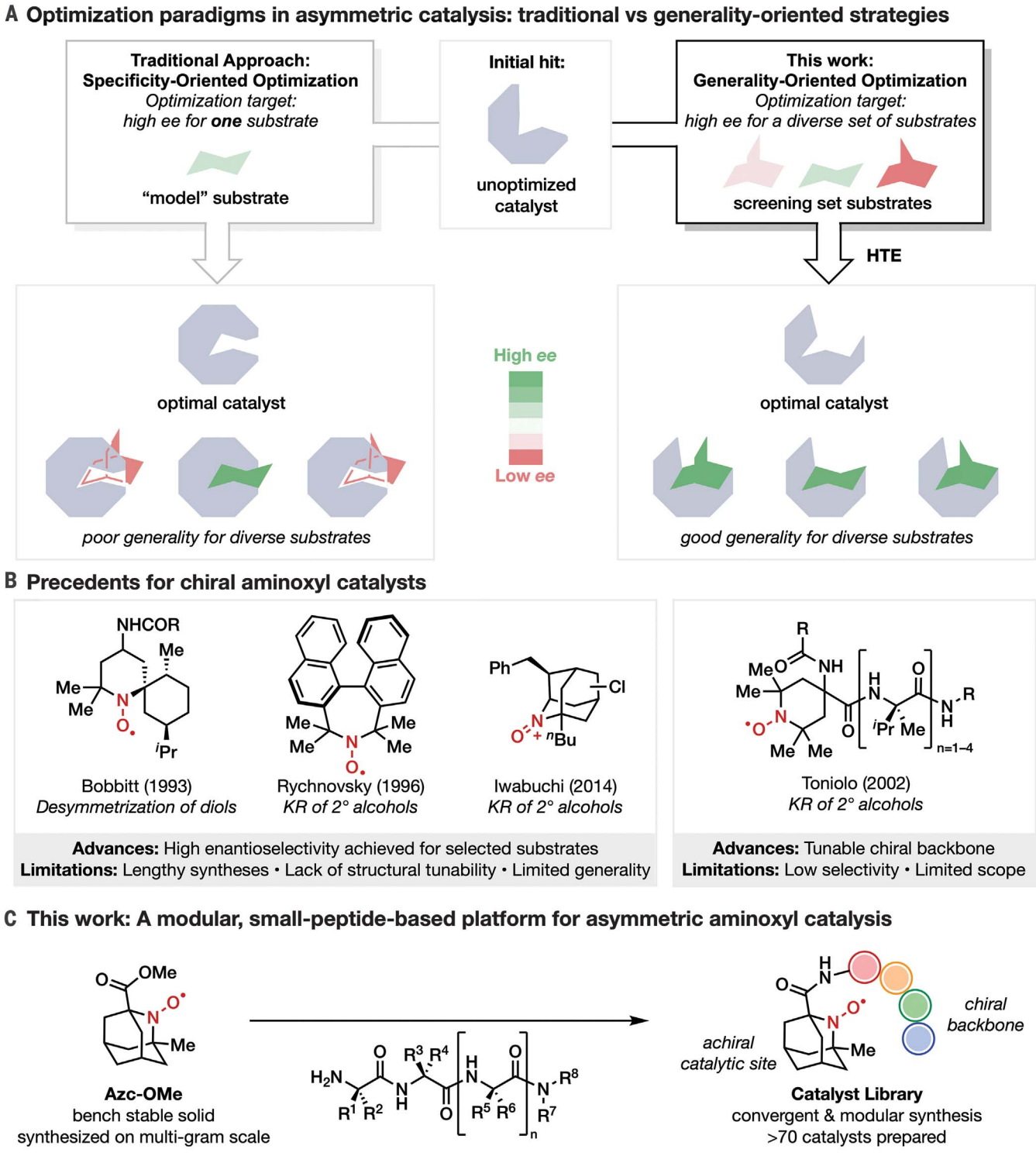

Fig. 1. A generality-oriented optimization strategy for enantioselective catalysis with peptidyl aminoxyl radicals. (**A**) Optimization paradigms in asymmetric catalysis: traditional versus generality-oriented strategies. (**B**) Precedents for chiral aminoxyl and oxoammonium catalysts (*12*, *19*, *20*, *22*). (**C**) This work: A modular, small-peptide-based platform for aminoxyl asymmetric catalysis. **Azc-OMe** was accessed in seven steps with a single chromatographic separation.

result underscores the challenge of identifying highly selective catalysts that tolerate a broad scope when focusing on a singular substrate during catalyst optimization.

Generality-oriented catalyst optimization guided by median *ee*

Aiming for a more broadly applicable method, we assessed a diverse library of peptide scaffolds with high-throughput experimentation (HTE) using 24-well plate parallel screening and gas chromatography analysis (supplementary materials). Using this workflow, we discuss

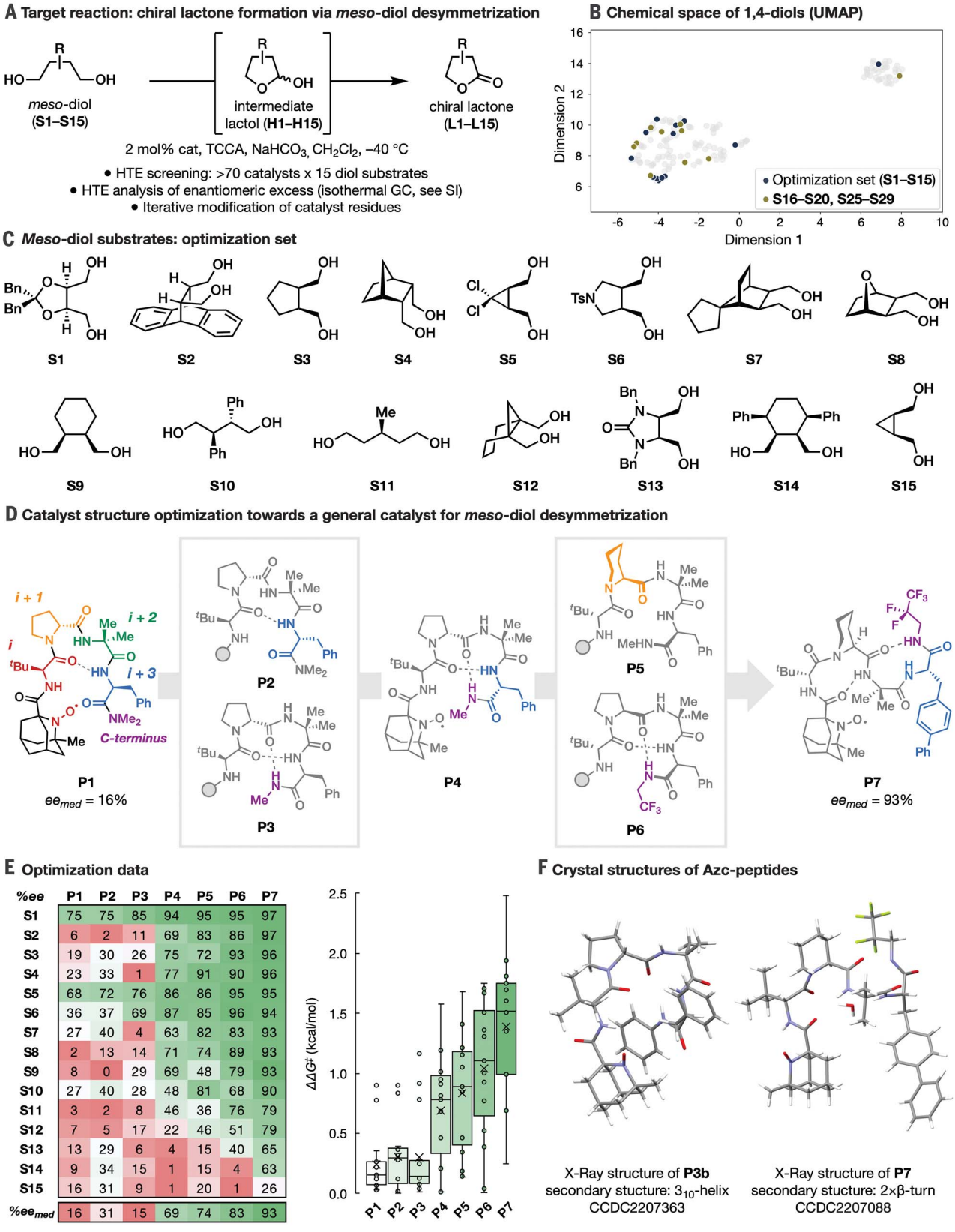

%ee	P1	P2	P3	P4	P5	P6	P7
S1	75	75	85	94	95	95	97
S2	6	2	11	69	83	86	97
S3	19	30	26	75	72	93	96
S4	23	33	1	77	91	90	96
S5	68	72	76	86	86	95	95
S6	36	37	69	87	85	96	94
S7	27	40	4	63	82	83	93
S8	2	13	14	71	74	89	93
S9	8	0	29	69	48	79	93
S10	27	40	28	48	81	68	90
S11	3	2	8	46	36	76	79
S12	7	5	17	22	46	51	79
S13	13	29	6	4	15	40	65
S14	9	34	15	1	15	4	63
S15	16	31	9	1	20	1	26
%ee_med	16	31	15	69	74	83	93

Fig. 2. Generality-oriented optimization through combinatorial screening of catalysts with a substrate library and iterative modification of catalyst structure. (**A**) Chiral lactone formation through *meso*-diol desymmetrization. (**B**) Chemical space of *meso*-1,4-diols defined by using Mordred descriptors and a uniform manifold approximation and projection (UMAP) with molecular fingerprints of commercial *meso*-1,4-diols from a Reaxys search. (**C**) *meso*-Diol substrates: optimization set. (**D**) Catalyst structure optimization. (**E**) Optimization data and box and whisker chart for the calculated $\Delta\Delta G^{\ddagger}$ for the optimization data. (**F**) Crystal structures of peptides **P3b** and **P7**.

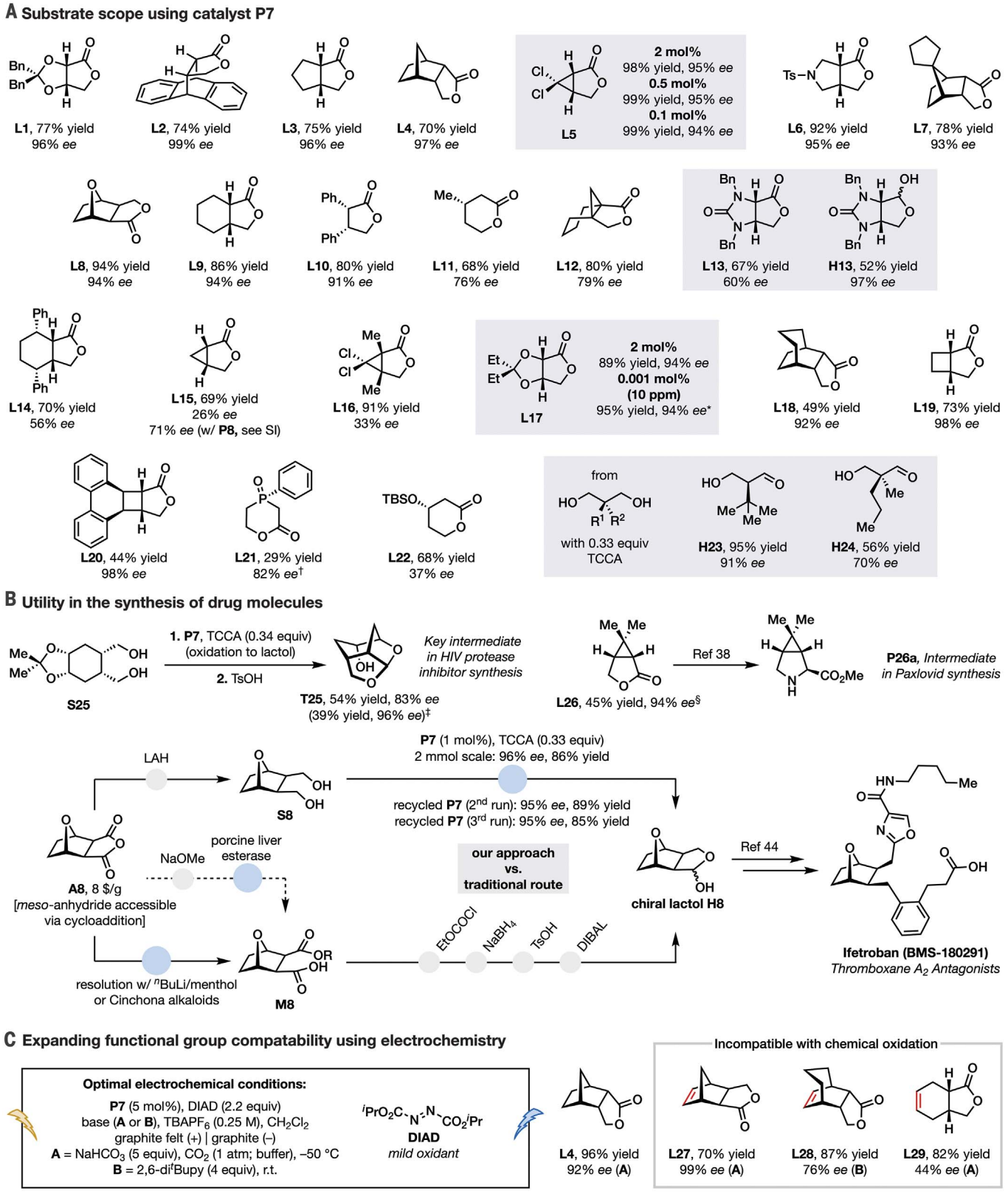

Fig. 3. Substrate scope. (**A**) Substrate scope by using catalyst **P7**. (**B**) Utility in the synthesis of drug molecules. (**C**) Expanding functional group compatibility by using electrochemistry. Absolute stereochemistry was assigned by analogy to **L1**, **L4**, and **L6**. *0.001 mol % **P7**, 96 hours, −50°C, then 2 mol % ACT, 0.3 equiv TCCA, room temperature (r.t.), 6 hours. †Isolated as the methyl ester after SiO_2 catalyzed methanolysis. ‡After trituration with pentane; §10 mol % **P7**.

the data obtained with a given catalyst in terms of the ee_{med}, which served as the primary optimization objective; excellent conversion and clean reaction profiles for each substrate enabled a narrow focus of the optimization on enantioselectivity. Substrate selection was guided by mapping the chemical space of commercially available *meso*-1,4-diols to ensure diversity of the screening set (Fig. 2B). This was accomplished by computing molecular descriptors of all commercially available *meso*-diols and applying dimensionality reduction techniques (supplementary materials) (*29*, *30*). This analysis revealed two clusters of diols, with the larger cluster representing disubstituted *meso*-diols, and the smaller cluster consisting of a distinct group of 2,2,3,3-tetrasubstituted 1,4-diols. From this collection of compounds, 14 structurally diverse substrates with a variety of functionalities were included in the optimization set. On the basis of their relative position within the uniform manifold approximation and projection (UMAP) and synthetic accessibility, we settled on eight monocyclic (**S1**, **S3**, **S5**, **S6**, **S9**, and **S13** to **15**) and five polycyclic (**S2**, **S4**, **S7**, **S8**, and **S12**) substrates with various ring sizes, as well as one acyclic diol (**S10**), to function as our representative set of diols (Fig. 2C). Additionally, we included a 1,5-diol (**S11**) to further increase diversity in the optimization set.

With this set of model substrates, we then evaluated catalysts as a function of their constituent residues (Fig. 2D). Beginning with **P1** (ee_{med} = 16%), two single-point changes exhibited increases in *ee*: inversion of stereochemistry at *i*+*3* (**P2**) provided ee_{med} of 31%, and replacement of the NMe_2 group at the C terminus with NHMe (**P3**) provided an ee_{med} of 15% but displayed considerable improvement for three substrates (**S1**, **S6**, **S9**). Auspiciously, **P3b**, an analog of **P3** maintaining the key C-terminal secondary amide, was crystalline, allowing determination of the secondary structure by means of single-crystal x-ray diffraction analysis (Fig. 2F); rotating-frame nuclear Overhauser effect correlation spectroscopy (ROESY) nuclear magnetic resonance (NMR) confirmed that the peptide adopts a 3_{10}-helical motif in solution (*31*). The confluence of changes leading to **P2** and **P3** from **P1** was found to be beneficial; **P4**, possessing both the optimized relative stereochemical configuration of **P2** and the NHMe C terminus of **P3**, provided a considerable enhancement in selectivity, with an ee_{med} of 69% (**P4**). Further modifications to **P4** showed that two additional point changes furnished substantial enhancement in ee_{med}: Replacement of the five-membered proline (Pro) with the six-membered homolog pipecolic acid (Pip) at *i* + 1 (**P5**) led to an increase of ee_{med} to 74%; concurrently, the inclusion of the fluorinated $NHCH_2CF_3$ substituent at the C-terminal position resulted in peptide **P6**, which greatly outperformed catalysts with other C termini, exhibiting an ee_{med} of 83%. Catalyst **P7**, which combined the Pip residue found in **P5** with an elongated polyfluorinated C terminus ($NHCH_2C_2F_5$) and a change to biphenylalanine (Bip) at *i* + 3, gave a further boost of ee_{med} to 93%, with 10 of 15 substrates showing >90% *ee*, and an additional four substrates displaying *ee* > 60%. Single-crystal x-ray diffraction analysis and ROESY NMR were also performed on **P7**, revealing that both the aminoxyl radical and the active oxoammonium forms of the catalyst share secondary structural features. The solid-state structure of **P7** shows a departure from the 3_{10}-helix observed in **P3b**, displaying instead two successive β-turns (Fig. 2F) (*32*). Because it appears that multiple secondary structures can contribute to effective enantioinduction, attributing high enantioselectivity to a singular stereochemical model may not reflect the behavior of an ensemble. Several conformationally distinct transition states are plausible—an emerging feature of flexible, highly effective enantioselective catalysts (*32*, *33*) and a likely basis for the observed high selectivity across a diverse collection of *meso*-diols.

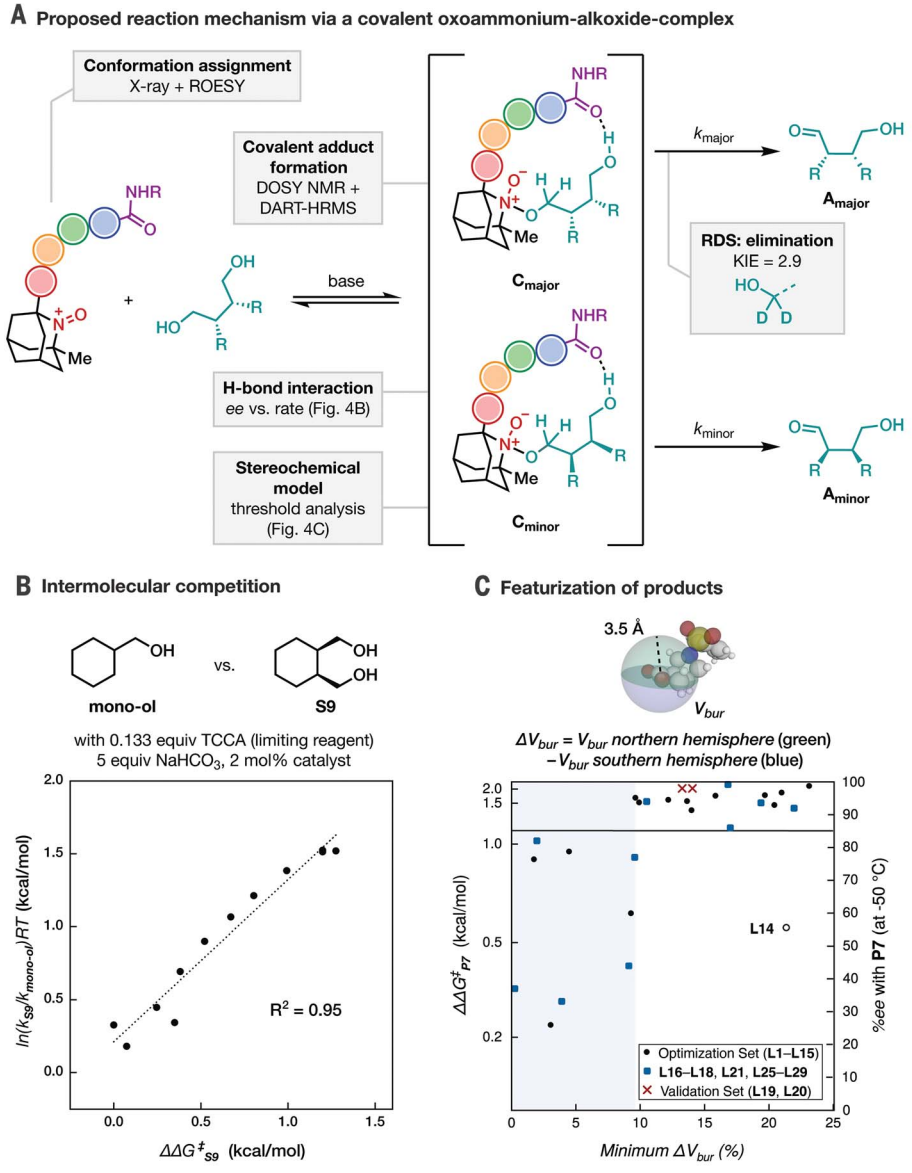

Fig. 4. Mechanistic analysis. (**A**) Proposed reaction mechanism through a covalent oxoammonium-alkoxide complex. (**B**) Intermolecular competition studies. (**C**) Featurization of products (1,3-diols **S23** and **S24** were omitted from the analysis because they do not form lactones upon oxidation). A discussion of **L14** as a false positive is available in the supplementary materials.

Substrate scope and synthetic applications

We then carried out the desymmetrization on a synthetically relevant scale (0.2 mmol) using the optimal catalyst **P7** (Fig. 3A). In addition to the 15 original substrates selected for the optimization campaign, we included a panel of *meso*-diols with varying chain lengths (1,3-, 1,4-, and 1,5-diols) and skeletal arrangements that further sample the chemical space (Fig. 2B and 4C) to define the scope and limitations of this method. We found that ketal-protected erythronic acid γ-lactones **L1** and **L17** were formed in good yields and excellent enantioenrichment. Polycyclic diols were efficiently desymmetrized (**L2**, **L4**, **L7**, **L8**, and **L18**), providing valuable precursors for pharmaceuticals and chiral ligands (*34*–*36*). A suite of fused bicyclic lactones was also efficiently synthesized. For example, cyclopentane lactone **L3** and fungistatic cyclohexane lactone **L9** (*37*) were formed with 96% *ee* and 94% *ee*, respectively, and cyclobutane-derived diols provided the corresponding [5.4.0]-fused bicyclic lactones **L19** and **L20** in 98% *ee*. Evaluation of cyclopropane diols revealed a requirement for substitution on the ring for high selectivity; unsubstituted **L15** was accessed in only 26% *ee*; however, dichloro- and dimethylcyclopropane lactones **L5** and **L26** were produced with excellent enantioselectivity, the latter of which is a key intermediate in the preparation of numerous important targets, including COVID drug nirmatrelvir (Paxlovid) (Fig. 3B) (*38*, *39*). Parenthetically, a structurally distinct catalyst **P8** (supplementary materials, section 4) was identified that provided **L15** in 71% *ee*, further highlighting the advantage of the modular catalyst screening platform. Pyrrolidine-bearing **S6** was desymmetrized with excellent yield (92%) and selectivity (95% *ee*). Skeletally distinct linear 1,4-diols were also good substrates in this reaction; lactone **L10** was obtained in 80% yield and 91% *ee*. Tetrasubstituted diols were also compatible, with bicyclic substrate **S12** yielding a [4.3.1]-propellane that featured two contiguous quaternary stereogenic centers in 80% yield and 79% *ee*; tetrasubstituted lactone **L16**, however, was obtained in only 33% *ee*.

To further evaluate the limit of our approach, we performed the desymmetrization of prochiral linear 1,5-diol and 1,3-diols. Diol **S11**, bearing a methyl group at the central carbon, was transformed to δ-lactone **L11** with 76% *ee*, providing access to a monomer for a biodegradable isotactic polymer (*40*). The catalyst was also competent in desymmetrization of a prochiral-at-phosphorous 1,5-diol, affording lactone **L21** in 82% *ee*. An additional 1,5-diol exhibited lower selectivity, with **L22** being enriched to only 37% *ee*. Notably, 1,3-diols, which were completely absent from the substrate screening set, also provided high enantioselectivities, yielding mono-oxidized β-hydroxy aldehydes as valuable synthetic precursors. 2-*tert*-butyl diol **S23** was efficiently desymmetrized in both excellent yield (95%) and enantioselectivity (91% *ee*). A disubstituted 1,3-diol **S24** yielded an α-quaternary β-hydroxy aldehyde (**H24**), a challenging motif to access in high enantioenrichment through alternative methods, differentiating methyl and propyl groups in 70% *ee*.

In the above cases, the reported enantiomeric excess reflects the selectivity in the initial desymmetrization step rather than that of the subsequent lactol oxidation because (i) for most substrates, we observed minimal stereochemical control of the second oxidation by the catalyst, and (ii) we carried out the reaction with an excess of TCCA to ensure full conversion of the intermediate lactol to the lactone product. However, we observed in two cases unusual kinetic resolution in either of the two oxidation steps, which was leveraged to improve enantioselectivity by decreasing the loading of TCCA. For example, diphenylcyclohexyl diol **S14**, which throughout optimization gave poor selectivities, was desymmetrized up to 56% *ee*. Slow interconversion between enantiomeric chair conformations may be responsible for the decreased enantioselectivity because using only 0.17 equiv of TCCA (0.5 oxidizing equivalents) resulted in enhanced enantioselectivity of the corresponding lactol (72% *ee*). Similarly, urea **L13**, a valuable intermediate in the chemical synthesis of biotin (*41*), was initially accessed in 60% *ee*. We observed a kinetic resolution of intermediate **H13**, which preferentially oxidized the minor enantiomer to **L13** and allowed for the isolation of **H13** in 52% yield and 97% *ee* when using 0.17 equiv TCCA. The oxidation of racemic hemiacetal **H13** by using **P7** revealed a selectivity factor of 8.3 for the oxidation to the lactone **L13**.

Catalyst **P7** exhibited high chemoselectivity for oxidation of diols over lactols (Fig. 4B), which enabled direct access to these valuable synthons by lowering the oxidant stoichiometry. We showcased this method in the concise formal synthesis of two pharmaceutical candidates, improving on previous routes in step count. Thus, we obtained tricyclic **T25**, a key intermediate in the synthesis of an HIV protease inhibitor (*42*), through oxidation of acetonide **S25** followed by one-pot acid-mediated transacetalization in 54% overall yield with 83% *ee* (Fig. 3B). In a second example, we obtained lactol **H8**, an intermediate in the synthesis of thromboxane receptor antagonist ifetroban (*43*, *44*) that is currently in clinical trials, on 2 mmol scale in 96% *ee* and 86% yield through an expedient two-step process from commercial *meso*-acid anhydride **A8**. By contrast, traditional syntheses required enantioselective methanolysis of **A8** to form monoester **M8** followed by a sequence of redundant functional group interconversions and redox manipulations (*45*, *46*).

To establish the upper limit of catalytic turnover, we surveyed decreased catalyst loadings using diethyl ketal **S17** and found that even 0.001 mol % catalyst (10 parts per million; 200,000% decrease from standard 2 mol % conditions) promoted the reaction without any loss in yield or enantioselectivity. Thus, **P7** achieved ~1.2×10^5 turnovers, which to our knowledge is the highest number recorded for an oligopeptide organocatalyst (*47*). The catalyst could also be recycled (>95% isolated from the reaction as the **P7** derived hydroxylamine) and reused (up to three times), as shown in the synthesis of **H8**, further demonstrating the potential practicality of the reported protocol (Fig. 3B and supplementary materials, section 13).

Electrochemical oxidation to enhance functional group compatibility

The optimal conditions established by using catalyst **P7** showed a broad scope with respect to the skeletal diversity of substrates, but the reaction generality was somewhat limited by compatibility of ancillary functional groups with TCCA. Substrates containing alkenes were chlorinated, resulting in diminished yields (0 to 25%). Such products are nonetheless useful synthetic intermediates; for example, unsaturated **L27** was leveraged in the preparation of another thromboxane-A_2 antagonist (*48*). To address this issue, an electrochemical protocol was developed. The key was identification of a functional group-tolerant sacrificial oxidant that would not decompose sensitive substrates but would readily participate in the cathodic half reaction (*49*). In traditional anodic oxidation reactions, protic acids or alkyl halides are used as sacrificial oxidants (*50*), but these species proved incompatible with our reaction system, likely because of the liberation of Lewis basic anions during their cathodic reduction, which led to detrimental catalyst binding. Rapid screening by using parallel reactor HTe$^-$Chem led to the identification of two classes of oxidants that provided high yields and enantioselectivities: dialkyl azodicarboxylates and disubstituted peroxides. We found that diisopropyl azodicarboxylate (DIAD) proved to be optimal, providing products **L27** to **29** in good yields and high enantioselectivity, with DIAD reduced to innocuous diisopropyl hydrazine-1,2-dicarboxylate (Fig. 3C). In this case, we used either an organic base 2,6-di-*tert*-butylpyridine or an inorganic buffer that consisted of $NaHCO_3$ and CO_2.

Mechanistic studies

We next conducted studies to gain understanding of the mechanistic underpinnings of the observed substrate promiscuity and high

enantioselectivity (Fig. 4A). We examined the composition of the resting state of the catalyst using in situ diffusion-ordered spectroscopy (DOSY) NMR experiments and direct analysis in real time (DART) high-resolution mass spectrometry, showing the formation of an oxoammonium-alkoxide complex (**C**) between the catalyst and the diol substrate. Further kinetic isotope effect (KIE) studies support that the rate-determining step of the reaction is a Cope-elimination from the resting state adduct to provide the desymmetrized aldehyde intermediates (**A**) (*13*). Subsequently, we performed a suite of kinetic experiments to probe additional catalyst-substrate interactions. Intermolecular competition studies between diol **S9** and mono-ol, cyclohexylmethanol, established excellent correlation [coefficient of determination (R^2) = 0.95] between the enantioenrichment of **L9** ($\Delta\Delta G^{\ddagger}$) and the relative reaction rate of **S9** versus mono-ol [$\ln(k_{diol}/k_{mono\text{-}ol})RT$] (Fig. 2B). More enantioselective catalysts showed a higher degree of selectivity toward diol over mono-ol oxidation with up to a 26-fold rate difference. These findings depict a structure in which the spectator alcohol participates in hydrogen bonding with a functional group on the peptide backbone (Fig. 4A), in addition to the covalent association of the reacting alcohol and the oxoammonium catalytic unit.

Consistent with this, product features can be used to quantitatively predict when a substrate should perform well in this reaction. We initially applied a classification algorithm to the optimization set (**S1** to **S15**) (*51*). Using a cutoff value of 85% *ee* under standard reaction conditions, substrates can be binned on the basis of the difference between the buried volumes (V_{bur}%) of each face of the lactone structure (Fig. 4C). We refined this analysis using the additional test set diols (**S16** to **S18**, **S21, S22**, and **S25** to **S29**), which were selected with the goal of assessing substrate diversity. These diols covered a broad range of ΔV_{bur}%, which revealed that substrates with a minimum ΔV_{bur}% at 3.5 Å of greater than 9.6% provide excellent enantioselectivity. We used diols **S19** and **S20** that contain a cyclobutane backbone not represented in the training data to validate the model; both **S19** and **S20** were correctly predicted to give high enantioselectivity, which suggests that this classification model can be used prospectively.

Taken together, positing that the diol motif provides multipoint binding with the catalyst, the substituents on the substrate backbone impart steric differentiation between the opposing diastereomeric transition states, providing a basis for the observed high enantioselectivity. This model of stereoinduction is simple yet highly effective, requiring only two alcohol groups that are necessary for the reaction and a relatively small steric distinction (ΔV_{bur}% = 9.6) between the two enantiotopic faces of the diol. The enantioselectivity of the reaction is otherwise insensitive to the chain length, skeletal constitution, functional groups, and other structural factors. This stereochemical model serves as the basis of the observed substrate generality.

REFERENCES AND NOTES

1. T. P. Yoon, E. N. Jacobsen, *Science* **299**, 1691–1693 (2003).
2. E. N. Jacobsen, A. Pfaltz, H. Yamamoto, *Comprehensive Asymmetric Catalysis* (Springer, 1999), vol. I to III.
3. D. A. Strassfeld, R. F. Algera, Z. K. Wickens, E. N. Jacobsen, *J. Am. Chem. Soc.* **143**, 9585–9594 (2021).
4. C. C. Wagen, S. E. McMinn, E. E. Kwan, E. N. Jacobsen, *Nature* **610**, 680–686 (2022).
5. X. Gao, H. B. Kagan, *Chirality* **10**, 120–124 (1998).
6. T. Satyanarayana, H. B. Kagan, *Adv. Synth. Catal.* **347**, 737–748 (2005).
7. H. Kim *et al*., *Nat. Commun.* **10**, 770 (2019).
8. K. Burgess, H.-J. Lim, A. M. Porte, G. A. Sulikowski, *Angew. Chem. Int. Ed.* **35**, 220–222 (1996).
9. A. J. Metrano *et al*., *Chem. Rev.* **120**, 11479–11615 (2020).
10. Y. Wang *et al*., *Chem. Rev.* **121**, 12384–12444 (2021).
11. P. A. Lichtor, S. J. Miller, *Nat. Chem.* **4**, 990–995 (2012).
12. F. Formaggio *et al*., *Chemistry* **8**, 84–93 (2002).
13. J. E. Nutting, M. Rafiee, S. S. Stahl, *Chem. Rev.* **118**, 4834–4885 (2018).
14. J. C. Siu, J. B. Parry, S. Lin, *J. Am. Chem. Soc.* **141**, 2825–2831 (2019).
15. J. M. Bobbitt, C. BrüCkner, N. Merbouh, in *Organic Reactions* (Wiley, 2010); pp. 103–424.
16. S. Nagasawa, Y. Sasano, Y. Iwabuchi, *Heterocycles* **105**, 61–114 (2022).
17. M. F. Semmelhack, C. R. Schmid, *J. Am. Chem. Soc.* **105**, 6732–6734 (1983).
18. F. Wang, M. Rafiee, S. S. Stahl, *Angew. Chem. Int. Ed.* **57**, 6686–6690 (2018).
19. Z. Ma, Q. Huang, J. M. Bobbitt, *J. Org. Chem.* **58**, 4837–4843 (1993).
20. K. Murakami *et al*., *J. Am. Chem. Soc.* **136**, 17591–17600 (2014).
21. M. Tomizawa, M. Shibuya, Y. Iwabuchi, *Org. Lett.* **11**, 1829–1831 (2009).
22. S. D. Rychnovsky, T. L. McLernon, H. Rajapakse, *J. Org. Chem.* **61**, 1194–1195 (1996).
23. Y. Iwabuchi, *Chem. Pharm. Bull.* **61**, 1197–1213 (2013).
24. H. Shimizu, S. Onitsuka, H. Egami, T. Katsuki, *J. Am. Chem. Soc.* **127**, 5396–5413 (2005).
25. T. Suzuki, K. Morita, Y. Matsuo, K. Hiroi, *Tetrahedron Lett.* **44**, 2003–2006 (2003).
26. Y. Kashiwagi *et al*., *Chem. Commun.* **2003**, 114–115 (2003).
27. A. Borissov *et al*., *Chem. Soc. Rev.* **45**, 5474–5540 (2016).
28. H. Tanaka, Y. Kawakami, K. Goto, M. Kuroboshi, *Tetrahedron Lett.* **42**, 445–448 (2001).
29. D. Zell *et al*., *J. Am. Chem. Soc.* **143**, 19078–19090 (2021).
30. S. K. Kariofillis *et al*., *J. Am. Chem. Soc.* **144**, 1045–1055 (2022).
31. E. G. Hutchinson, J. M. Thornton, *Protein Sci.* **3**, 2207–2216 (1994).
32. A. J. Metrano *et al*., *J. Am. Chem. Soc.* **139**, 492–516 (2017).
33. J. M. Crawford, E. A. Stone, A. J. Metrano, S. J. Miller, M. S. Sigman, *J. Am. Chem. Soc.* **140**, 868–871 (2018).
34. B. M. Trost, B. Vidal, M. Thommen, *Chemistry* **5**, 1055–1069 (1999).
35. T. Kametani, T. Suzuki, S. Kamada, K. Unno, *J. Chem. Soc., Perkin Trans. 1* **1981**, 3101–3105 (1981).
36. S. Hagishita, K. Seno, *Chem. Pharm. Bull. (Tokyo)* **37**, 327–335 (1989).
37. T. Olejniczak, F. Boratyński, A. Białońska, *J. Agric. Food Chem.* **59**, 6071–6081 (2011).
38. B. Thierry, D. Patrice, France patent FR2972453 (A1) (Minakem, France, 2012).
39. L. E. Löffler, C. Wirtz, A. Fürstner, *Angew. Chem. Int. Ed.* **60**, 5316–5322 (2021).
40. C. Zhang *et al*., *ACS Sustain. Chem.& Eng.* **4**, 4396–4402 (2016).
41. M. Seki, Y. Takahashi, *Org. Process Res. Dev.* **25**, 1950–1959 (2021).
42. A. K. Ghosh *et al*., *J. Med. Chem.* **63**, 4867–4879 (2020).
43. L. Rosenfeld, G. J. Grover, C. T. Stier Jr., *Cardiovasc. Drug Rev.* **19**, 97–115 (2001).
44. R. N. Misra *et al*., *J. Med. Chem.* **36**, 1401–1417 (1993).
45. J. Das, M. F. Haslanger, J. Z. Gougoutas, M. F. Malley, *Synthesis* **1987**, 1100–1103 (1987).
46. Y. Chen, S.-K. Tian, L. Deng, *J. Am. Chem. Soc.* **122**, 9542–9543 (2000).
47. F. Giacalone, M. Gruttadauria, P. Agrigento, R. Noto, *Chem. Soc. Rev.* **41**, 2406–2447 (2012).
48. F. Lieb, U. Niewöhner, D. Wendisch, *Liebigs Ann. Chem.* **1987**, 607–615 (1987).
49. J. Rein *et al*., *ACS Cent. Sci.* **7**, 1347–1355 (2021).
50. X. Dong, J. L. Roeckl, S. R. Waldvogel, B. Morandi, *Science* **371**, 507–514 (2021).
51. S. H. Newman-Stonebraker *et al*., *Science* **374**, 301–308 (2021).

ACKNOWLEDGMENTS

We thank K. D. Logan, L. Alperstein, and J. S. K. Ho for substrate preparation; F. Menges (Yale University) for high-resolution mass spectrometry analysis of peptides; and H. Yoon (AbbVie), Z. Girvin (Pfizer), T. Morack (Yale University), and J. Robins (Yale University) for helpful discussion. **Funding:** This work was supported by National Institute of General Medical Sciences grant R01GM134088 (J.R., S.B.Z., J.C.S., and S.L.); National Institute of General Medical Sciences grant R35GM132092 (S.D.R., O.C.L., and S.J.M.); National Institute of General Medical Sciences grant R35GM136271 (M.A.H. and M.S.S.); ERP-Fellowship from the Studienstiftung des Deutschen Volkes (J.R.); Wiberg Graduate Research Fellowship in Chemistry (S.D.R.); National Science Foundation Graduate Research Fellowship Program (O.C.L. and S.B.Z.); and American Cancer Society–Roaring Fork Valley Research Circle Postdoctoral Fellowship PF-21-089-01-ET (M.A.H.). This work made use of the Cornell University NMR Facility, which is supported in part by the NSF through MRI award CHE-1531632. The computational portion of this work was supported by the Center for High Performance Computing (CHPC) at the University of Utah. **Author contributions:** J.R. and S.D.R. contributed equally and are listed in alphabetical order. O.C.L. and S.B.Z. contributed equally and are listed in alphabetical order. S.L., S.J.M., and M.S.S. supervised the project. J.R., S.D.R., O.C.L., S.B.Z., and J.C.S. performed synthetic experiments. J.R. and M.A.H. performed mechanistic and computational studies. B.Q.M. collected and analyzed x-ray crystallography data. The manuscript was written by S.D.R., J.R., M.A.H., M.S.S., S.J.M., and S.L. and was edited and approved by all authors. **Competing interests:** The authors declare that they have no competing interests. **Data and materials availability:** Full x-ray structural data are available free of charge from the Cambridge Crystallographic Data Centre (CCDC) under deposition nos. 2207088, 2207089, 2207090, 2207091, and 2207363. All other data are available in the main text or the supplementary materials.

SUPPLEMENTARY MATERIALS

science.org/doi/10.1126/science.adf6177
Materials and Methods
Supplementary Text
Figs. S1 to S52
Tables S1 to S43
References (*52*–*91*)
Data S1 and S2

Submitted 2 November 2022; resubmitted 16 February 2023
Accepted 29 March 2023
10.1126/science.adf6177